A Letters Journal Exploring the Frontiers of Physics

December 2018

EPL, **124** (2018) 64003 www.epljournal.org
doi: 10.1209/0295-5075/124/64003

Effect of anti-Langmuir adsorption on spreading in porous media

C. Rana[1], M. Mishra[2,3] and A. De Wit[1]

[1] *Université libre de Bruxelles (ULB), Nonlinear Physical Chemistry Unit - 1050 Brussels, Belgium*
[2] *Department of Mathematics, Indian Institute of Technology Ropar - Rupnagar-140001, Punjab, India*
[2] *Department of Chemical Engineering, Indian Institute of Technology Ropar - Rupnagar-140001, Punjab, India*

received 11 August 2018; accepted in final form 13 December 2018
published online 8 January 2019

PACS 47.35.-i – Hydrodynamic waves
PACS 47.20.Gv – Viscous and viscoelastic instabilities
PACS 47.10.A- – Mathematical formulations

Abstract – When given solutes are transported in porous media flows, various propagation regimes can be observed depending on the adsorption isotherms. We perform numerical simulations to investigate the influence of an anti-Langmuir adsorption isotherm (overloading isotherm) on the spreading of a miscible solute-rich slice in a porous medium. Selecting the characteristic scaling of the solute concentration appropriately, the dynamics of the anti-Langmuir adsorbed solute is studied in the pure diffusion-convection conditions as well as under the influence of viscous fingering. The similarities and differences between the spreading of Langmuir and anti-Langmuir adsorbed miscible slices are analysed as a function of the parameters of the problem.

Introduction. – The propagation of fluids through porous media is receiving focused attention because of applications related to enhanced oil recovery (EOR) techniques [1], chromatography [2] and contaminant transport [3]. For instance, in EOR techniques a carefully designed polymer buffer solution must be injected to minimise the effect of mixing that otherwise would lead to lesser effective recovery. Similarly, in chromatography techniques during the transport of solutes their mixing and dispersion can result in poor sensitive chromatograms which hampers the separation process. The situation becomes even more complicated when the solute present in the fluid interacts with the porous medium via adsorption [4]. Adsorption processes involve an array of phenomena which can alter the distribution of solutes between and among the constituent phases and interfaces of subsurface systems. The interchange of mass associated with such processes impacts the fate and transport of many inorganic and organic substances [5]. For instance, in chromatography, the solute component gets adsorbed on the surface of the porous medium which plays a role in the separation of the components. Also in applications related to enhanced oil recovery the component to be extracted can in some cases stick to the porous surface, which affects the yield of the extraction [2,6]. Thus, the understanding of the influence of adsorption on the transport of the solute is of fundamental importance.

The adsorption process follows the reversible adsorption-desorption step

$$A_m \underset{k_d}{\overset{k_a}{\rightleftharpoons}} A_s. \tag{1}$$

Here A_m and A_s represent the solute molecules in the mobile and stationary phases where their concentrations are equal to $\tilde{c}_m$ and $\tilde{c}_s$, respectively, while k_a and k_d are the adsorption and desorption kinetic constants. The relation between the stationary and mobile phase concentrations is given by the adsorption isotherm which can be linear or nonlinear. We briefly describe the linear, Langmuir and anti-Langmuir isotherms.

Linear isotherm. The linear isotherm is the simplest adsorption case, for which the concentration $\tilde{c}_s$ of the solute in the stationary adsorbed phase is directly proportional to its concentration $\tilde{c}_m$ in the mobile phase:

$$\tilde{c}_s = K\tilde{c}_m, \tag{2}$$

where $K = k_a/k_d$ is the equilibrium constant of the adsorption-desorption equilibrium. It is graphically represented in fig. 1(a). The solute retention is characterized by the retention factor $k = FK$, where $F = V_s/V_m = (1-\epsilon_{tot})/\epsilon_{tot}$ is the phase ratio of the volumes V_s and V_m of the stationary and mobile phases, where ϵ_{tot} is the total porosity or void volume fraction of the porous medium.

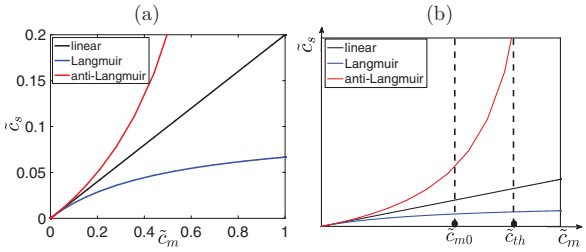

Fig. 1: (Colour online) (a) Linear, Langmuir, and anti-Langmuir adsorption isotherms. (b) Threshold $\tilde{c}_{th}$ and initial $\tilde{c}_{m0}$ mobile phase concentrations used in the model.

Langmuir isotherm. The Langmuir isotherm, is a nonlinear isotherm characterised by a saturation behaviour due to a reduction in the rate of increase of the stationary phase concentration when the liquid/mobile phase concentration increases [4]. The Langmuir isotherm is typically observed in the case of a monolayer saturation of the available adsorption sites on the porous medium. The Langmuir isotherm is expressed as

$$\tilde{c}_s = \frac{K\tilde{c}_m}{1+\tilde{b}\tilde{c}_m}, \tag{3}$$

where $\tilde{b} = K/\tilde{c}_{sat}$ with $\tilde{c}_{sat}$ the saturation concentration on the porous matrix [2]. The stationary phase concentration gradually reaches the saturation concentration $K/\tilde{b}$ of the porous medium when the mobile phase concentration $\tilde{c}_m \to \infty$ (see fig. 1(a)).

Anti-Langmuir isotherm. The anti-Langmuir isotherm is an overloading isotherm often used to describe convex downward isotherms in gas-liquid or liquid-solid equilibria [7]. In this isotherm, the stationary phase concentration starts increasing towards infinity when increasing the mobile phase solute concentration (fig. 1(b)). Such isotherms are typically obtained in the case of a cooperative effect of the adsorbate favouring further adsorption. This behaviour can be expressed by the following equation [8]:

$$\tilde{c}_s = \frac{K\tilde{c}_m}{1-\tilde{b}\tilde{c}_m}. \tag{4}$$

This model assumes that there is an infinite amount of adsorbate in the stationary phase when the concentration in the mobile phase is $1/\tilde{b}$, which is an unrealistic situation. Note that for the anti-Langmuir isotherm, the parameter $\tilde{b}$, although similar to that used in the Langmuir isotherm, does not have the physical meaning of a saturation capacity. This is because the stationary phase concentration can grow indefinitely, thus $\tilde{b}$ is an empirical parameter. Since the anti-Langmuir isotherm is valid for $\tilde{c}_m \leq 1/\tilde{b}$, the concentration $\tilde{c}_{th} = 1/\tilde{b}$ is defined as the threshold concentration of the column. In the adsorption process, the determination of the isotherm, *i.e.*, the relation between the stationary and mobile phase, is a difficult task during the design and optimization of many preparative chromatographic processes and in oil recovery processes [9]. While in a significant number of situations, the adsorption behaviour of a binary mixture can be modelled with linear or Langmuir isotherm, there are numerous exceptions [10]. For instance, in supercritical fluid chromatographic processes due to the complex nature of interaction between the adsorbent and adsorbate, the isotherms are nonlinear with a complex chromatographic behaviour. To describe such complex behavior using a single-component adsorption isotherm, one may need to use an anti-Langmuir isotherm (AL-isotherm) [11].

In addition to adsorption processes, a fingering instability can also occur if the sample is of different viscosity from that of the carrier fluid [12–14]. This leads to an increased spreading of the sample in space and time. The spatio-temporal evolution of the adsorbed solute concentration then results from a highly nonlinear coupling between the solute adsorption and the transport processes like dispersion and convection. Numerous studies have already analysed the coupling of linear and Langmuir adsorption with viscous fingering, both experimentally [2,6,15,16] and numerically [17–19]. As a result of the nonlinear adsorption (Langmuir or anti-Langmuir type), the velocity of the solute propagation depends on the concentration of the solute itself. This can lead to either contraction of the concentration front known as shock layer or expansion of the concentration front known as rarefaction, depending on the initial concentration profile of the solute [10,20,21]. For the Langmuir adsorption there are a few theoretical studies [19,22–24] that examine the influence of adsorption on spreading of the solute. However, the anti-Langmuir adsorption isotherm is not yet reported in the theoretical community. The main problem in studying the influence of the anti-Langmuir isotherms is the difficulty of implementing the isotherm in the mass balance equations. This problem occurs because of the divergence of the stationary phase solute concentration as $\tilde{c}_m$ approaches the threshold value $\tilde{c}_{th}$. The main objective of this article is to implement the anti-Langmuir adsorption isotherm in a mathematical model in order to understand its influence on solute spreading. This article also calls attention to the potentially critical role of anti-Langmuir adsorption on the spreading of the solute in the presence of viscous fingering.

Mathematical model. – The porous medium is assumed to be isotropic, homogeneous with constant permeability K_p. In this medium, an incompressible fluid of dynamic viscosity $\tilde{\mu}_1$ displaces a finite size sample of miscible fluid of dynamic viscosity $\tilde{\mu}_2$ at a uniform velocity $\tilde{U}$. The displaced fluid is a solution of a given solute, which is retained on the porous matrix following adsorption-desorption steps. The local equilibrium between the solute phases (mobile and stationary phase) is supposed to set in instantaneously. The dynamic viscosity of the system

is governed by the mobile phase solute concentration $\tilde{c}_m$, through an exponential relation as $\tilde{\mu}(\tilde{c}_m) = \tilde{\mu}_1 e^{R(\tilde{c}_m/\tilde{c}_0)}$, where $R = \ln(\tilde{\mu}_2/\tilde{\mu}_1)$ is the log mobility ratio. The mathematical model used to study the propagation pattern of finite width sample is the equilibrium dispersive model, the detailed description of which can be found in the literature [2]. The governing equations are as follows:

$$\tilde{\underline{\nabla}} \cdot \tilde{\underline{u}} = 0, \tag{5}$$

$$\tilde{\underline{\nabla}}\tilde{p} = -\frac{\tilde{\mu}(\tilde{c}_m)}{K_p}\tilde{\underline{u}}, \tag{6}$$

$$\frac{\partial \tilde{c}_m}{\partial \tilde{t}} + F\frac{\partial \tilde{c}_s}{\partial \tilde{t}} + (\tilde{\underline{u}} \cdot \tilde{\underline{\nabla}})\tilde{c}_m = \tilde{D}\tilde{\nabla}^2\tilde{c}_m. \tag{7}$$

The evolution of the velocity field $\tilde{\underline{u}} = (\tilde{u}, \tilde{v})$ of the incompressible fluid is described by two-dimensional Darcy's law (eq. (6)). The solute transport is governed by the mass balance equation (7) for the concentration of the solute, $\tilde{p}$ is the pressure, $\tilde{\mu}$ is the dynamic viscosity of the fluid, $\tilde{D}$ is the molecular diffusion coefficient.

After substituting $\tilde{c}_s$ from the nonlinear anti-Langmuir isotherm relation (4), the mass balance equation (7) reduces to

$$\frac{\partial}{\partial \tilde{t}}\left(1 + \frac{k}{(1 - \tilde{b}\tilde{c}_m)}\right)\tilde{c}_m + \tilde{\underline{u}} \cdot \tilde{\underline{\nabla}}\tilde{c}_m = \tilde{D}\tilde{\nabla}^2\tilde{c}_m, \tag{8}$$

where $k = FK$ is the retention parameter. The Langmuir case can be analysed using the isotherm (3) instead.

The initial mobile phase concentration $\tilde{c}_{m0} = \tilde{c}_m(x, 0)$ is assumed to be

$$\tilde{c}_{m0} = \tilde{c}_m(\tilde{x}, 0) = \begin{cases} \tilde{c}_{th}/\alpha, & \text{for } |\tilde{x}| \leq \tilde{W}_s/2, \\ 0, & \text{elsewhere.} \end{cases} \tag{9}$$

Here $\tilde{W}_s$ is the width of the injected sample and $\alpha > 1$. In this approach, we assume that the initial solute concentration in the mobile phase is below the threshold value $\tilde{c}_{th}$ (see fig. 1(b)). In this way we overcome the intrinsic divergence of the anti-Langmuir adsorption isotherm while maintaining the original physics. The specific choice of the α value is not crucial. We have checked that results are robust provided α is large enough for the concave part of the anti-Langmuir isotherm to have an effect.

Nondimensional model. Equations (5), (6) and (8) are nondimensionalised by taking $\tilde{U}, \tilde{D}/\tilde{U}$ and $\tilde{D}/\tilde{U}^2$ as characteristic velocity, length and time, respectively. The viscosity of the displacing fluid $\tilde{\mu}_1$ is used to scale viscosity and $\tilde{\mu}_1\tilde{D}/K_p$ to scale pressure. The solute concentration is nondimensionalized with the threshold mobile phase concentration in the displacing fluid, *i.e.*, $\tilde{c}_{th}$ while the nonlinear adsorption parameter $\tilde{b}$ is scaled by $1/\tilde{c}_{th}$. The dimensionless governing equations in the moving frame

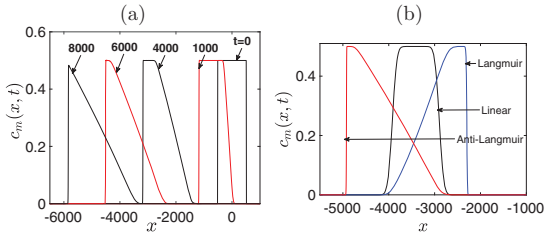

Fig. 2: (Colour online) (a) Concentration profiles $c_m(x, t)$ for $b = 1, k = 1, R = 0$ at different times. (b) Concentration profiles for linear, Langmuir and anti-Langmuir adsorbed solutes at time $t = 6000$.

$x = \tilde{x} - \tilde{U}\tilde{t}$ are

$$\underline{\nabla} \cdot \underline{u} = 0, \tag{10}$$

$$\underline{\nabla}p = -\mu(c_m)(\underline{u} + \underline{e}_x), \tag{11}$$

$$\left(1 + \frac{k}{(1 - bc_m)^2}\right)\frac{\partial c_m}{\partial t} - \frac{k}{(1 - bc_m)^2}\frac{\partial c_m}{\partial x} + u \cdot \underline{\nabla}c_m = \nabla^2 c_m, \tag{12}$$

$$\mu(c_m) = e^{Rc_m}. \tag{13}$$

Here $\underline{e}_x$ is the unit vector in the axial direction. The nondimensional length and width of the computational domain are $L = UL_x/D$ and $L' = UL_y/D$, respectively. Equations (10)–(13) are numerically solved by using a Fourier pseudo spectral method for the simulation of the dynamics of the solute propagation [25,26]. The boundary conditions are assumed to be periodic in both axial and transverse directions. The numerical stability is attained for $\mathrm{d}x = \mathrm{d}y = 1$, $\mathrm{d}t = 0.1$. We fix here $\alpha = 2$, which sets the initial mobile phase concentration $c_m(x, 0) = 0.5, \forall x$.

Shock and rarefaction waves. – Let us first analyse the influence of the nonlinear isotherm properties on the spreading of the miscible slice in the absence of any VF instability, *i.e.*, for $R = 0$. In that case, the convective term in eq. (12) can be omitted and transport is analysed in 1D. The mass balance equation (12) for the adsorbed solute in one dimension reduces to

$$\left(1 + \frac{k}{(1 - bc_m)^2}\right)\frac{\partial c_m}{\partial t} - \frac{k}{(1 - bc_m)^2}\frac{\partial c_m}{\partial x} = \frac{\partial^2 c_m}{\partial x^2}. \tag{14}$$

The mass balance equation (14) for the anti-Langmuir isotherm can be used to derive the mass balance equation for the linear and the Langmuir cases as well. For instance, for $b = 0$, eq. (14) gives the transport equation for the linear isotherm and for $b < 0$ the equation represents the mass balance of the Langmuir isotherm. The concentration profile of the mobile phase of the solute undergoing anti-Langmuir adsorption with $R = 0$ is shown in fig. 2(a). The solute shows the formation of triangular profile with a highly dispersed frontal interface and a steepened rear interface. This kind of profile is a particular feature of an anti-Langmuir adsorbed solute [27].

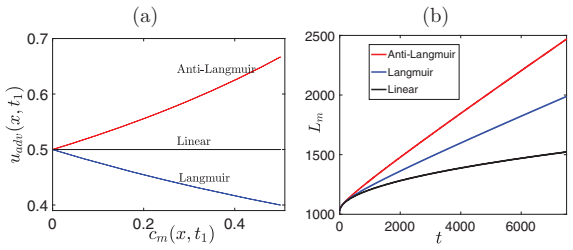

Fig. 3: (Colour online) (a) Local advection speed in the moving reference frame as a function of the local value of c_m at a given time for different adsorption isotherms. (b) Spreading length of the adsorbed solute for different adsorption isotherms.

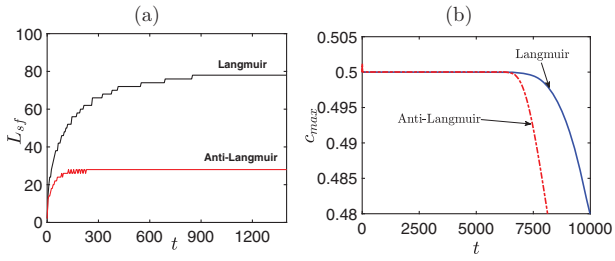

Fig. 4: (Colour online) (a) Spreading length of the shock front L_{sf} of the adsorbed solute for $R = 0, k = 1$ and $b = 1$, for Langmuir and anti-Langmuir adsorption. (b) The interaction time of the shock layer and rarefaction wave for Langmuir and anti-Langmuir adsorbed solutes.

This is due to the fact that when a finite slice is injected into the column, the step-up and step-down concentrations are the initial concentrations at the interfaces. Only one of the step concentration retains its shape while the other one gives rise to a highly diffused profile. The reduced dispersion regime observed at the rear interface of the sample depicts the self-sharpening phenomenon of the anti-Langmuir adsorption, whereas the broadened frontal interface features the rarefaction phenomenon [28]. For a while the band maintains a flat top of concentration c_0, with sharpening on one side and an expanding profile on the other side. The propagation of the sharpened interface and the maximum point of concentration on the continuous profile are such that the width of the flat top decreases constantly while the bandwidth widens. When the flat top collapses the maximum concentration decreases, *i.e.*, when the shock layer and the rarefaction wave interact, the right-angled triangular profiles are obtained (see fig. 2(a) at time $t = 8000$).

To quantify theoretically to what extent the properties of the anti-Langmuir isotherm differ from those of the Langmuir and the linear isotherms, the solute concentration profiles are compared for these 3 cases in fig. 2(b). The profiles are quite different from each other which shows that the solute band is strongly influenced by the properties of the adsorption isotherm. For instance, the linear adsorption isotherm shows symmetric diffused interfaces whereas for the Langmuir and anti-Langmuir cases each interface is propagating differently. For the Langmuir isotherm, the front part of the sample develops a shock layer while a rarefaction wave is formed at the rear interface of the sample [19]. On the contrary, for the anti-Langmuir isotherm the front part builds up a rarefaction layer while the other interface is a shock layer. The behaviour of the interfaces varies because of the dependence of the advection velocity on the solute concentration. From eq. (14), the advection velocity of the adsorbed solute in the moving reference frame (in the upstream direction) is given by $u_{adv} = \frac{\frac{k}{(1-bc_m)^2}}{1+\frac{k}{(1-bc_m)^2}}$ and is plotted in fig. 3(a) for linear ($b = 0$), Langmuir ($b < 0$) and anti-Langmuir ($b > 0$) isotherms. For the linear isotherm, the advection speed is independent of the concentration, therefore both interfaces of the finite slice show a symmetric distribution. However, for the Langmuir and anti-Langmuir isotherms the advection speed varies with the solute concentration. In a moving reference frame and for Langmuir, high concentration zones move slower than lower concentration ones (in the upstream direction), therefore the concentration profile shows a widening at the rear interface and sharpening at the frontal interface [19,25]. Whereas, for an anti-Langmuir isotherm, the high concentration zones move faster, thus the widening is at the frontal interface and the rear one shows a steepened profile. Therefore, all three profiles are different from each other and are strongly affected by the concentration dependent advection speed. These 3 different types of propagation profiles are well reported in the experimental literature [2] and match very well with our simulation results.

In order to get more insight into the spreading dynamics of the solute slice, we evaluate the spreading length of the solute, L_m, measured as the width of the interval for which the solute concentration $c_m(x,t) > 0.001$ [13]. Figure 3(b) shows that the spreading length of the Langmuir and the anti-Langmuir isotherms is larger than that of the linear one, this is due to the formation of the rarefaction zones in the nonlinear adsorption cases. However, the spreading length of the anti-Langmuir adsorbed solute is the largest among all. This is because in that case the rarefaction wave is formed in the direction of the flow, thus the advection speed of the high concentration zone is further enhanced which results in a larger spreading.

Since, the onset of the shock layer and its interaction with the rarefaction wave are the two important features of both Langmuir and anti-Langmuir isotherms, we further compare both profiles by computing the onset time of the shock layer and the interaction time of the two waves for both isotherms. For the evaluation of the onset time of the shock layer, we compute the spreading length of the shock layer zone L_{sf} (frontal interface in the Langmuir isotherm and rear interface in the anti-Langmuir one) as the width of the interval for which $0.001 < c_m < 0.5$ (fig. 4(a)). The saturation of L_{sf}, corresponds to the onset of the shock layer. Clearly, from fig. 4(a), we see that the shock

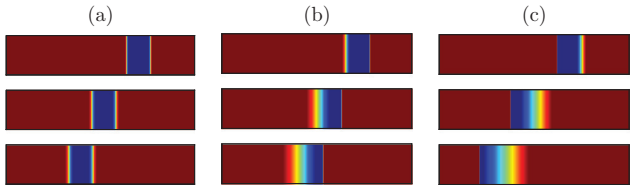

Fig. 5: (Colour online) Adsorbed solute concentration fields for (a) linear, (b) Langmuir, (c) anti-Langmuir isotherms with $R = 0, k = 1, b = 1$ at times $t = 1000$, 4000, 6000.

layer develops earlier for the anti-Langmuir adsorbed solute than for the Langmuir adsorbed solute. Moreover, since L_{sf} for the anti-Langmuir case is smaller than L_{sf} for the Langmuir one, it also confirms that the anti-Langmuir shock layer zones are narrower than the Langmuir ones.

After some time there is an interaction of the shock layer and of the rarefaction zone for both Langmuir and anti-Langmuir isotherms. To quantify the time at which both interfaces start to interact, we plot c_{max}, *i.e.*, the maximum concentration of the solute peak as a function of time in fig. 4(b). Initially, the maximum concentration is constant and equals 0.5. It starts decreasing after some time and the starting time of the decrease represents the interaction time of the two interfaces. It is seen that for the anti-Langmuir isotherm the peak concentration starts decreasing earlier than for the Langmuir isotherm. So the anti-Langmuir isotherm has an earlier interaction of the two fronts in comparison to the Langmuir one. Thus, we can conclude that the triangular profiles are obtained earlier for the anti-Langmuir isotherm.

In the following section, we further quantify theoretically the spreading dynamics of the overloading anti-Langmuir isotherm in the presence of a viscous fingering instability.

Viscously unstable displacement. – The viscous fingering (VF) instability can come into play when there is a given viscosity contrast between the displaced and invading fluids. Let us now analyse how the VF dynamics develops on both the shock layer and rarefaction zones of the anti-Langmuir and Langmuir profiles. To understand the difference in fingering dynamics at both interfaces, we recall that to develop VF at the rear interface the less viscous fluid must displace the more viscous slice, *i.e.*, $R > 0$, while to have VF at the frontal interface $R < 0$ [29]. In the absence of adsorption, the VF dynamics (for both $R > 0$ and $R < 0$) are the same as long as the two interfaces do not interact. Before describing the cases with $R \neq 0$, fig. 5 analyses the 2-dimensional evolution of the solute undergoing linear, Langmuir and anti-Langmuir adsorption when $R = 0$. Clearly, the linear case shows a symmetric evolution at both fronts, whereas for the Langmuir and anti-Langmuir cases, the highly diffused front is the rarefaction zone and the less diffused one is the shock layer zone. 1D concentration profiles such as those shown in figs. 2 and 3 can be obtained from the transverse average

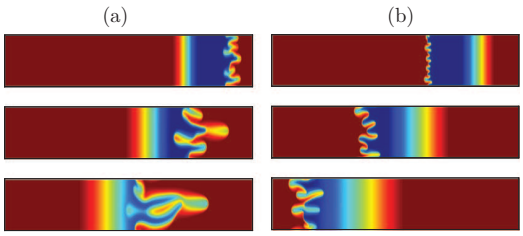

Fig. 6: (Colour online) Concentration of the adsorbed solute in the presence of a VF instability in the shock layer zone for $k = 1, b = 1$ (a) Langmuir isotherm with $R = -3$ and (b) anti-Langmuir isotherm with $R = 3$ at times $t = 2000$, 4000, 6000.

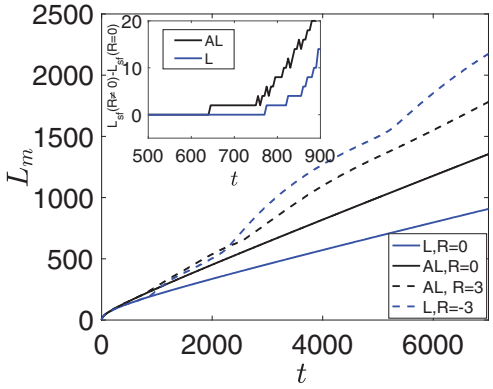

Fig. 7: (Colour online) Spreading length L_m for the anti-Langmuir isotherm with $R = 3$ and the Langmuir isotherm with $R = -3$ for $k = 1, b = 1$. Inset: change in the spreading length of the shock layer zone L_{sf} for $R \neq 0$ from $R = 0$ for both isotherms.

of the two-dimensional solute concentration computed as $\bar{c}_m(x,t) = \frac{1}{L'}\int_0^{L'} c_m(x,y,t)\mathrm{d}y$. Let us now analyze the effect of varying the log-mobility ratio R on the propagation pattern of the adsorbed solute for the Langmuir and anti-Langmuir cases.

Comparison of VF in the shock layer zone. VF can be observed in the shock layer zone for the anti-Langmuir case when $R > 0$ and for the Langmuir one when $R < 0$. As shown in fig. 6, the fingering dynamics is different in these two cases. The fingers for the Langmuir isotherm are able to intrude more into the carrier fluid in comparison to the anti-Langmuir one. To quantify this effect, we compute the spreading length of the adsorbed solute L_m and the onset time of VF. The spreading length L_m for the fingered zone at the shock layer interface is shown for both adsorption cases in fig. 7. Clearly, under the influence of VF, L_m is larger for the Langmuir isotherm than for the anti-Langmuir one. This is in contrast to the spreading dynamics for $R = 0$ where L_m for anti-Langmuir is larger than for the Langmuir case (solid lines in fig. 7). In order to compute the onset time of VF, we evaluate the spreading length of the unstable shock layer zone L_{sf}. The deviation of L_{sf} for $R \neq 0$ from $R = 0$ gives the onset time of VF. In the inset of fig. 7, we see that VF sets in as soon

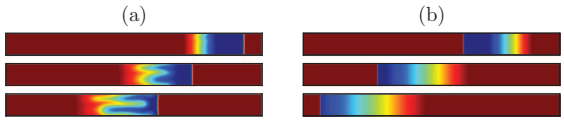

Fig. 8: (Colour online) Concentration fields for the unstable rarefaction zone with $k = 1, b = 1$ for (a) $R = 4$ with Langmuir adsorption, (b) $R = -4$ with anti-Langmuir adsorption at time $t = 3000$, 6000, 8000.

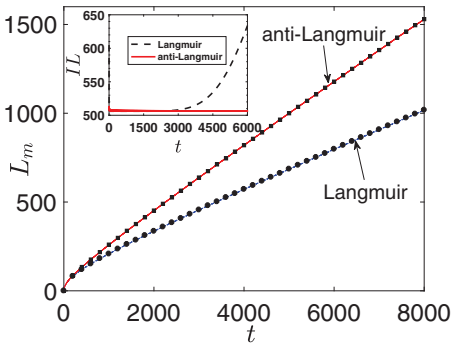

Fig. 9: (Colour online) Spreading length L_m for the anti-Langmuir isotherm with $R = -4$ and the Langmuir isotherm with $R = 4$ for $k = 1, b = 1$. Here the marked lines are for L_m with $R = 0$ which are overlapping L_m with $R \neq 0$. Inset: corresponding interfacial length IL of the adsorbed solute plug for the Langmuir and anti-Langmuir isotherms.

as $L_{sf}(R \neq 0) - L_{sf}(R = 0) > 0$. The onset time of VF for the anti-Langmuir case is smaller than the Langmuir one, since the shock front of the anti-Langmuir adsorbed solutes is steeper than the Langmuir one, *i.e.*, L_{sf} of the anti-Langmuir isotherm $< L_{sf}$ for the Langmuir isotherm (see fig. 4). Therefore, the viscosity gradient at the shock front for the anti-Langmuir isotherm is larger than the Langmuir isotherm which favours the earlier onset of VF.

Comparison of VF in the rarefaction zone. VF of the rarefaction front can be observed for the anti-Langmuir case when $R < 0$ and for the Langmuir one when $R > 0$. Figure 8 shows the concentration fields for the Langmuir with $R = 4$ and the anti-Langmuir with $R = -4$. The rarefaction front of the Langmuir adsorbed solute features an instability, whereas no VF patterns are observed for the anti-Langmuir case. Since, the rarefaction zone of the anti-Langmuir adsorbed solute is more diffused than the Langmuir one (see fig. 9), the highly diffused rarefaction front of the anti-Langmuir does not let the convective forces dominate. As a result VF is suppressed by the rarefaction front of the anti-Langmuir adsorbed solute.

From fig. 9 we see that the spreading length of the unstable rarefaction interfaces ($R \neq 0$) is the same as for $R = 0$ until the two interfaces start interacting. Therefore, the fingering dynamics observed at the rarefaction zone of the Langmuir adsorbed solute are not able to intrude through the diffused rarefaction interface. Thus, in order to compute the onset of VF at the rarefaction front we evaluate the interfacial length of the sample which changes with the onset of VF. The interfacial length [30] of the rarefaction front is evaluated for both isotherms as $IL = \int_0^{L'} \int_0^{L} [(\frac{\partial c_m}{\partial x})^2 + (\frac{\partial c_m}{\partial y})^2] \mathrm{d}x\mathrm{d}y$ and is plotted in the inset of fig. 9. The deviation of IL from the initial value (512) features the onset time of VF. Clearly the Langmuir isotherm has an onset of VF at time around $t = 3000$, whereas no deviation is observed for the anti-Langmuir isotherm. Therefore, we can conclude that the rarefaction fronts of the anti-Langmuir and Langmuir adsorbed solutes behave differently with regard to VF.

Conclusion. – We have theoretically investigated the spreading dynamics in a porous medium of a miscible slice containing a solute undergoing anti-Langmuir adsorption. An appropriate choice of the scaling parameter of the initial solute concentration in the anti-Langmuir isotherm allows the study of the dispersive and VF regime of this overloading isotherm. For the dispersive regime the solute concentration profiles obtained for linear, Langmuir and anti-Langmuir isotherms match well with those described in the existing experimental and theoretical literature [8,20]. The results obtained show that the propagation pattern for the Langmuir and the anti-Langmuir isotherms features occurrence of a shock layer and of a rarefaction zone in both cases but their interaction time and the spreading are different. The properties of the adsorption isotherms thus significantly affect the propagation pattern of the adsorbed solute. The adsorption isotherms also significantly influence viscously unstable flows. In the presence of viscosity contrast, there is an earlier onset of VF at the shock layer front of the anti-Langmuir adsorbed solute but the spreading length of the Langmuir adsorbed one is larger. On the other hand, if a viscosity contrast can destabilise the rarefaction zone, no VF patterns are seen for the anti-Langmuir case. The results obtained show that the onset of VF and the dynamic evolution of the fingers are largely dependent on the concavity or convexity of the adsorption isotherm.

* * *

We thank M. Martin and W. De Malsche for fruitful discussions. CR and ADW acknowledge the financial support of BELSPO and FRS-FNRS PDR CONTROL programme. MM acknowledges the support from MATRICS, SERB, Government of India (grant No. MTR/2017/000283).

REFERENCES

[1] Dominguez J. G. and Willhite G. P., *Soc. Pet. Eng. J.*, **17** (1977) 111.
[2] Guiochon G., Felinger A., Shirazi D. G. and Katti A. M., *Fundamentals of Preparative and Nonlinear Chromatography* (Academic Press) 2006.
[3] Abriola L. M., *Rev. Geophys.*, **25** (1987) 125.
[4] Ruthven D. M., *Principles of Adsorption and Adsorption Processes* (Wiley) 1984.

[5] Weber W. J. jr., McGinley P. M. and Katz L. E., *Water Resour*, **25** (1991) 499.
[6] Krumrine P. H., Falcone J. S. jr. and Campbell T. C., *Soc. Pet. Eng. J.*, **22** (1982) 503.
[7] Cavazzini A., Bardin G., Kaczmarski K., Szabelski P., Al-Bokari M. and Guiochon G., *J. Chromatogr. A*, **957** (2002) 111.
[8] Gritti F., Piatkowski W. and Guiochon G., *J. Chromatogr. A*, **978** (2002) 81.
[9] Hsu C.-T., Chang C.-H. and Lin S.-Y., *Langmuir*, **13** (1997) 6204.
[10] Weber W. J. jr. and Rumer R. R. jr., *Water Resour. Res.*, **1** (1965) 361.
[11] Lübbert M., Brunner G. and Johannsen M., *J. Supercrit. Fluids*, **42** (2007) 180.
[12] Homsy G. M., *Annu. Rev. Fluid Mech.*, **19** (1987) 271.
[13] De Wit A., Bertho Y. and Martin M., *Phys. Fluids*, **17** (2005) 054114.
[14] Baroni M. P. M. A., De Wit A. and Rosa R. R., *EPL*, **92** (2010) 64002.
[15] Jamaloei B. Y. and Kharrat R., *Transp. Porous Media*, **81** (2010) 1.
[16] Edström L., Samuelsson J. and Fornstedt T., *J. Chromatogr. A*, **1218** (2011) 1966.
[17] Mishra M., Rana C., De Wit A. and Martin M., *J. Chromatogr. A*, **1297** (2013) 46.
[18] Vossoughi S., Smith J. E., Green D. W. and Willhite G. P., *Soc. Pet. Eng. J.*, **24** (1984) 56.
[19] Rana C. and Mishra M., *Phys. Fluids*, **29** (2017) 032108.
[20] Helfferich F. G. and Carr P. W., *J. Chromatogr.*, **629** (1993) 97.
[21] De Vault D., *J. Am. Chem. Soc.*, **65** (1943) 532.
[22] Zhu J., Ma Z. and Guiochon G., *Biotechnol. Prog.*, **9** (1993) 421.
[23] Sajonz P., Zhong G. and Guiochon G., *J. Chromatogr. A*, **786** (1997) 195.
[24] Zhu J. and Guiochon G., *J. Chromatogr.*, **636** (1993) 189.
[25] Rana C., *Computational study of adsorption effects on the miscible displacement in porous media*, PhD Thesis, Department of Mathematics, Indian Institute of Technology Ropar (2015).
[26] Tan C. T. and Homsy G. M., *Phys. Fluids*, **31** (1988) 1330.
[27] Golshan-Shirazi S. and Guiochon G., *J. Chromatogr. A*, **461** (1989) 19.
[28] Rhee H., Bodin B. F. and Amundson N. R., *Chem. Eng. Sci.*, **26** (1971) 1571.
[29] Mishra M., Martin M. and De Wit A., *Phys. Rev. E*, **78** (2008) 066306.
[30] Chen C.-Y. and Wang S.-W., *Int. J. Numer. Methods Heat Fluid Flow*, **11** (2001) 761.